analytical chemistry

pubs.acs.org/ac Article

Multiplexed Capillary-Flow Driven Immunoassay for Respiratory Illnesses

Jeremy S. Link, John O'Donnell-Sloan, Sierra Curdts, Brian J. Geiss, David S. Dandy, and Charles S. Henry*

Cite This: *Anal. Chem.* 2024, 96, 4111−4119 Read Online

ACCESS | Metrics & More | Article Recommendations | Supporting Information

ABSTRACT: Multiplexed analysis in medical diagnostics is widely accepted as a more thorough and complete method compared to single-analyte detection. While analytical methods like polymerase chain reaction and enzyme-linked immunosorbent assay (ELISA) exist for multiplexed detection of biomarkers, they remain time-consuming and expensive. Lateral flow assays (LFAs) are an attractive option for point-of-care testing, and examples of multiplexed LFAs exist. However, these devices are limited by spatial resolution of test lines, large sample volume requirements, cross-reactivity, and poor sensitivity. Recent work has developed capillary-flow microfluidic ELISA platforms as a more sensitive alternative to LFAs; however, multiplexed detection on these types of devices has yet to be demonstrated. In the aftermath of the initial SARS-CoV-2 pandemic, the need for rapid, sensitive point-of-care devices has become ever clearer. Moving forward, devices that can distinguish between diseases with similar presenting symptoms would be the ideal home diagnostic. Here, the first example of a multiplexed capillary-flow immunoassay device for the simultaneous detection of multiple biomarkers is reported. From a single sample addition step, the reagents and washing steps required for two simultaneous ELISAs are delivered to spatially separated test strips. Visual results can be obtained in <15 min, and images captured with a smartphone can be analyzed for quantitative data. This device was used to distinguish between and quantify H1N1 hemagglutinin (HA) and SARS-CoV-2 nucleocapsid protein (N-protein). Using this device, analytical detection limits of 840 and 133 pg/mL were obtained for hemagglutinin and nucleocapsid protein, respectively. The presence of one target in the device did not increase the signal on the other test line, indicating no cross-reactivity between the assays. Additionally, simultaneous detection of both N-protein and HA was performed as well as simultaneous detection of N-protein and human C-reactive protein (CRP). Elevated levels of CRP in a patient infected with SARS-CoV-2 have been shown to correlate with more severe outcomes and a greater risk of death as well. To further expand on the simultaneous detection of two biomarkers, CRP and N-protein were detected simultaneously, and the presence of SARS-CoV-2 N-protein did not interfere with the detection of CRP when both targets were present in the sample.

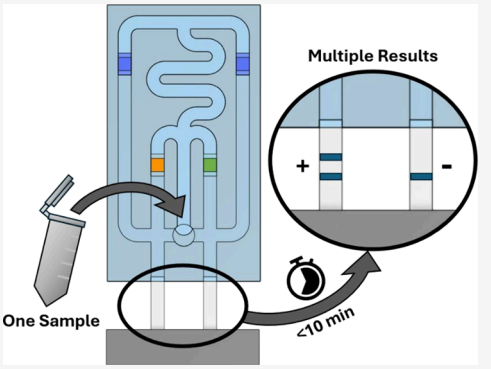

INTRODUCTION

The results of medical testing influence accurate diagnosis, prognosis, treatment, and timely discharge of patients from a medical facility. It follows that an early and affordable diagnosis is a crucial part of treatment. The sooner a patient can be diagnosed, the more effectively the diseases can be slowed, halted, or prevented.[1−3] Rapid testing for infectious diseases is also crucial for patient outcomes. The need for reliable testing has been a theme for decades, and the world seems to get a grim reminder of this need every few decades with new or reemerging infectious diseases. In recent history, HIV/AIDS in the 1980s to the present,[4,5] SARS-CoV in the early 2000s,[6] H1N1 in 2009,[7] and SARS-CoV-2 in early 2020 have posed great stress to diagnostic infrastructure. In both cases, communicable or noncommunicable, diagnostics that can detect multiple targets are preferred over single-target systems.

One of the most common ways to detect biological targets is enzyme-linked immunosorbent assays (ELISAs). Laboratory-based ELISAs are performed in 96-well microtiter plates. In this format, wells can be coated with a variety of capture proteins or antibodies. This spatial separation makes them ideal tools for multiplexing biological assays.[8] Unfortunately, ELISAs are time-consuming, requiring multiple pipetting steps and trained personnel to perform. These drawbacks hinder the ability of regular testing to occur, making it difficult to diagnose and treat patients.

Received: November 3, 2023
Revised: February 9, 2024
Accepted: February 14, 2024
Published: February 28, 2024

https://doi.org/10.1021/acs.analchem.3c04977
Anal. Chem. 2024, 96, 4111−4119

Point-of-care (POC) testing is an attractive alternative to traditional medical diagnostics in many ways. Reliable POC tests allow for faster time-to-result, more affordable and regular testing, and the opportunity for home testing and personalized medicine. Rapid, onsite, or POC testing is especially important in rural and resource-limited settings where a patient may have difficulty traveling to and from medical facilities.[9,10] In recent years, lateral flow assays (LFAs) have been a popular solution for POC diagnostics. LFAs consist of a series of membranes containing different reagents requires for a sandwich immunoassay to occur from a single sample addition with a gold nanoparticle-based readout.[11−13] LFAs can be used to assess environmental contaminants,[14,15] food safety,[16−18] and disease biomarkers.[17,19,20] There has also been considerable effort in developing multiplexed LFA devices. The simplest approach to multiplex LFAs is adding multiple test lines to a single test strip.[16,21−23] This allows for multiple targets to be captured and screened in a single strip but spatial constraints limit the number of analytes that can be targeted. Mathematical modeling has shown that test lines should be at least 2 mm apart for good detection.[24] Extending the length of the test strip membrane could increase room for additional test lines, but assay time would increase exponentially according to the Lucas−Washburn equation.[13,25] Microarrays of test spots offer another alternative for increasing the number of detection zones, but spatial resolution and cross-reactivity between signal and capture antibodies may still pose issues, although some products do exist in this format.[26−30] Spatially separating multiple test strip membranes reduces the number of test lines/targets per membrane. Successful devices have been designed where 10 individual LFA test strips radiate from a single sample inlet.[18,31] This removes the possibility of cross-reactivity between antibody pairs and spatially separates test lines but increases the total sample volume required to operate. Another example of multiple test strips on a single device comes from Han et al. In their work, stacked paper channels control sample and enhancer delivery to two separate test strips with three total test lines.[32] This device sequentially delivers gold nanoparticle conjugated signal antibodies followed by an enhancer solution.[32] While this delivery method is impressive, it does not allow for washing between steps, a highly desirable step for other applications like paper-based ELISAs.[32]

Paper-based ELISA has been used for more than a decade in various ways.[33,34] The simplest version of a paper-based ELISA replaces a 96-well plate with wax-patterned paper microwells.[33] While using paper may cut costs and improve portability, the manual pipetting steps required for this type of paper-based ELISA are still tedious. Several attempts have been made to simplify or automate the sample addition, washing, and regent delivery steps associated with an ELISA with the goal of making them more user-friendly.[35−37] While these examples are simpler than traditional ELISAs, they still require multiple steps after sample addition. Multiple automated, capillary-driven immunoassay devices have recently been developed that fully automate sample delivery, washing, and reagent delivery steps to test strips, but multiplexing on these devices has yet to be shown, to this point remaining a challenging future goal.[38−40]

In this work, we describe a capillary-driven device that passively delivers the reagent and washing steps associated with an ELISA to two spatially separated test strips with visual results in under 15 min from a single sample addition step. The device uses horseradish peroxidase (HRP) as a signal enzyme and 3,3′,5,5′-tetramethylbenzydine (TMB) as the amplification substrate. The device is assembled from an inexpensive double-sided adhesive and transparency film to create the microfluidic front end that leads to two nitrocellulose test strips. The channels of the device are oriented in such a way that, after sample addition, the sample, signal antibody, wash steps, and substrate are delivered to two separate test strips simultaneously. The device is also designed so that reagents for one target will never interact with reagents from the other side of the device. This separation prevents cross-reactivity that may occur between the capture and signal antibodies from the other assay.

Multiplexed detection was shown in two motifs. The first demonstrates the device's ability to distinguish between two conditions. For this example of multiplexed detection, the device was used to distinguish between H1N1 and SARS-CoV-2 infections from a single sample. These two are of special interest because many of their symptoms (fever, muscle soreness, cough, headaches, nausea, etc.) are not specific to either disease, making it difficult to distinguish between the two solely on the symptoms a patient presents.[41] The device was optimized to detect hemagglutinin from H1N1 on one test strip and nucleocapsid protein (N-protein) from SARS-CoV-2 on the other. Initial optimization for the H1N1 assay was performed on a single-channel device that was developed in previous work.[42] Once conditions were chosen, dose−response curves were generated for H1N1 hemagglutinin and SARS-CoV-2 nucleocapsid protein (N-protein) on the multiplex device with detection limits of 840 and 133 pg/mL, respectively. The amount of SARS-CoV-2 N-protein found in blood and saliva from positive patients ranges from 1 to 1 × 10^5 pg/mL for the first 2 weeks after infection; our device is well within that range.[43] Although it is difficult to determine the hemagglutinin concentration in positive patients, other similar POC devices claim LODs of 0.23−29 ng/mL[44−46] To show the device's function in the complex sample matrix, devices were run in nasal swabs spiked with varying concentrations of N-protein or HA. Results for our device can be read visually in under 15 min and can be quantified with a smartphone.

The second motif of multiplexed detection is the simultaneous detection of two targets. To demonstrate this type of multiplexed detection, two examples are shown. First would be an example of a coinfection of SARS-CoV-2 and H1N1. Although coinfections of the two diseases are rare,[47,48] many cases have been reported, and the severity of patient outcomes is typically more severe and a higher risk of death.[49,50] To demonstrate simultaneous detection, devices were run with 5 and 100 ng/mL for both N-protein and HA simultaneously to show proof of concept for simultaneous detection of both viral proteins. To further demonstrate this concept, N-protein from SARS-CoV-2 and C-reactive protein (CRP) were also detected simultaneously. Elevated levels of CRP have been found in patients infected with SARS-CoV-2.[51,52] Consequently, it has been suggested that elevated levels of CRP could be used as a predictor for the severity of a patient's condition.[53] Therefore, simultaneously detecting a SARS-CoV-2 infection and quantifying the amount of CRP in the same sample may be useful for the decision-making of healthcare providers. For this example, samples containing N-protein at 50 ng/mL and varying amounts of CRP were run. There was no statistical difference in the signal from the N-

https://doi.org/10.1021/acs.analchem.3c04977
Anal. Chem. 2024, 96, 4111−4119

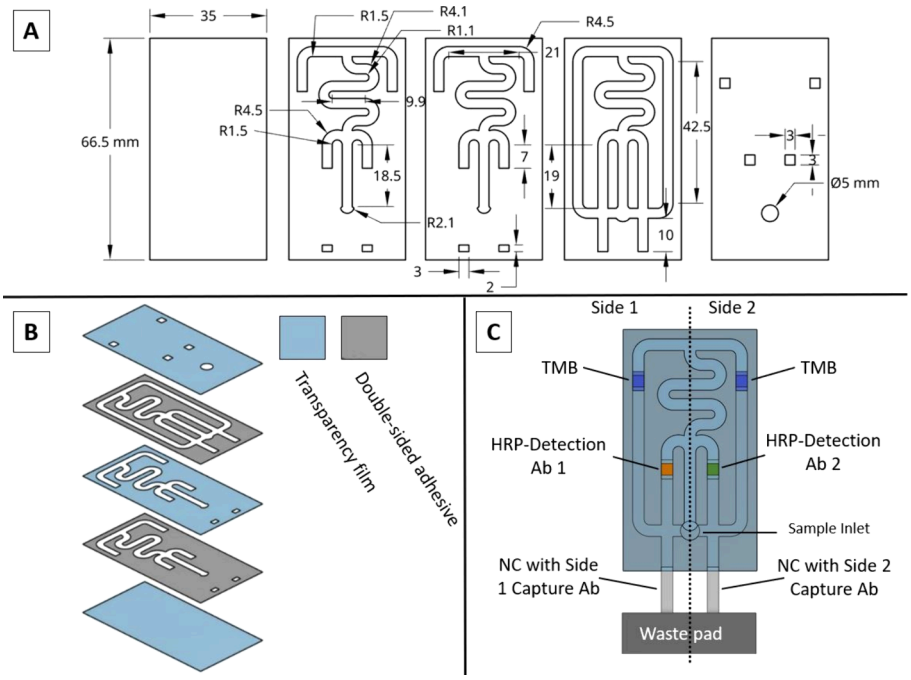

Figure 1. (A) Schematic with dimensions for each layer of the multiplexed CaDI. (B) Order in which the five layers are assembled. (C) Location of reagent pads and NC membranes containing TMB, HRP conjugated detection Ab for each assay, and NC with capture and control antibodies for each assay.

protein test strip, and the CRP test strip signal increased according to the increase in the CRP concentration. This work demonstrates the function and some potential applications of multiplexed, capillary-driven immunoassays for multiple biomarkers detected at clinically relevant concentrations.

MATERIALS AND METHODS

Nitrocellulose Test Strip Preparation. Nitrocellulose (NC) membranes (Vivid 90 LFNC, Pall, NY, USA) were stripped with test and control lines for each assay. For the N-protein test strips, 0.88 mg/mL for the anti-N-protein capture antibody (40143-MM08, Sino Biological, Beijing China) and goat antimouse control line antibody (AB6708, Abcam, Cambridge UK) was stripped using a BioSpot reagent printer (BioFluidix, Breisgau, Germany). For the HA test strips, 0.88 mg/mL for the anti-HA capture antibody (11055-RM10, Sino Biological) and goat antirabbit control line antibody (R1131, Millipore Sigma, Burlington MA, USA) was stripped. For the CRP test strips, 0.88 mg/mL anti-CRP capture antibody (PAB7943, Abnova, Taipei, Taiwan) and a CRP (30-AC05S, Fitzgerald, Acton MA, USA) control line were stripped. All test and control solutions also contained 4% glycerol and 4 mM trehalose for improved drying and longevity. All NC membranes were dried overnight in a desiccator before blocking with Stabilguard (SG01-1000, Surmodics Inc.) to prevent nonspecific adsorption to the membrane during the assay. The NC membranes were then cut into 15 × 3 mm^2 individual test strips using a CO_2 laser cutter (Epilog Zing, Golden, CO, USA). NC membranes were stored at 4 °C with a desiccant until used.

Reagent Pad Preparation. Glass fiber pads (GFDX203000, MilliporeSigma, Burlington, MA, USA) were used for both TMB and secondary antibody-HRP (2°Ab-HRP) pads, but the pretreatment and blocking conditions for each were slightly different. For the TMB pad, glass fiber sheets were completely submerged in a blocking solution containing 10 mM PBS (Thermo Scientific, Rockford, IL, USA), 3% sucrose, 0.5% Tween-20, and 0.1% thimerosal (MilliporeSigma) for 15 min. The sheets were removed from the solution and dried overnight at 37 °C before use. The dried, blocked membranes were then cut into 3 × 5 mm^2 reagent pads with a razor blade. TMB (TMBM-0100-01, Surmodics Inc., Eden Prairie, MN, USA) was pipetted onto the pads in 7.5 μL aliquots, and the aliquots were dried for 7−8 min between additions. After the final TMB addition, the pads were dried for 2 h before being assembled in the microfluidic device. For 2°Ab-HRP pads, blank glass fiber membranes were cut into 3 × 5 mm^2 reagent pads before any pretreatment. Aged casein was prepared following the procedures outlined in the work from Grant et al.[54] The aged casein was diluted to 0.5% in 10 mM PBS, and 15 μL was added to each 2°Ab-HRP pad in two 7.5 μL aliquots. The pads were dried for 7−8 min at 37 °C between additions and for an additional 30 min after the second. 2°Ab-HRP for the N-protein assay (40143-MM05-H, Sino Biological) and the HA assay (11055-RP07, Sino Biological) were diluted in a drying buffer designed for long-term stability.[55] Each diluted 2°Ab-HRP (5 μL) was added to separate treated pads and dried for 30 min at 37 °C before adding to the device. For the CRP assay, a conjugation kit (ab102890, Abcam, Cambridge, UK) was used to conjugate HRP to the detection antibody (MAB0421, Abnova). The manufacturer's protocol was followed for the conjugation kit, and the conjugated antibody was diluted to 20 μg/mL in drying buffer. The diluted Ab-HPR solution (5 μL) was added to treated glass fiber pads and dried for 30 min at 37 °C.

Device Assembly. Patterns for the device channels were designed in the CAD program, OnShape, and cut into alternating layers of the transparency film (3M 9984, Saint Paul, MN, USA) and double-sided adhesive (3M 467MP, Saint Paul, MN, USA) with a CO_2 laser cutter (Figure 1A,B). The

https://doi.org/10.1021/acs.analchem.3c04977
Anal. Chem. 2024, 96, 4111−4119

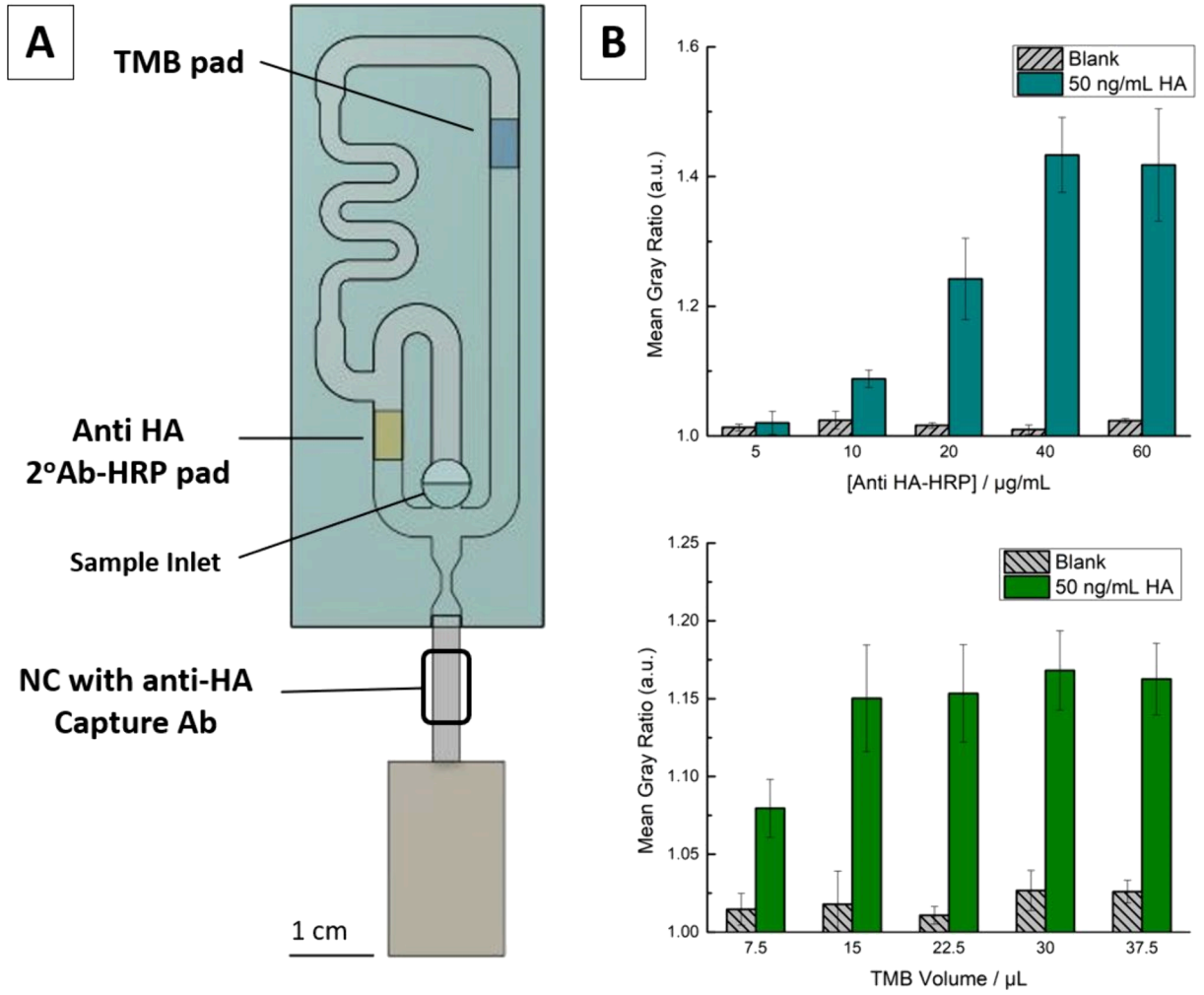

Figure 2. (A) The single NC CaDI device was used to optimize conditions for the influenza hemagglutinin assay. (B) The TMB volume was held at 30 μL, while the anti-HA 2°Ab-HRP concentration was varied. Following that, the anti-HA 2°Ab-HRP was held at 40 μg/mL, while the TMB volume dried on the TMB pad was varied.

first four layers of the device were assembled before the conjugate release pads were added. The final layer of the transparency film was added last, completing the hollow channels and securing the conjugate release pads in place. The devices were cut at the bottom to open the channels for the insertion of NC test strips. Conjugate release pads and NC test strip for the HA assay were assembled into the left half of the device, and N-protein pads and test stripwere assembled into the right side (Figure 1C). The entire device adhered to an adhesive backing, and a waste pad (CFSP223000, Millipore Sigma, Burlington, MA, USA) was pressed down to overlap with the end of the NC membrane.

Assay Optimization. The N-protein assay was previously studied extensively.[39,42] Therefore, the concentrations of 2°Ab-HRP and volume of the TMB substrate used in the N-protein assay were the same as from previous work.[42] The running buffer in which the sample was diluted was made using 1.5× stable peroxide buffer (Thermo Fisher Scientific, 34062) at pH 6.5 with 150 mM NaCl, 0.1% Igepal CA630, and 0.1% Tween-20. The influenza A H1N1 assay has never been performed on this type of capillary-driven immunoassay device (CaDI). To optimize the conditions for the HA side of the multiplex device, the HA assay was performed on the single-channel CaDI device outlined in previous work.[42] First, TMB volume was held constant at 30 μL while the 2°Ab-HRP concentration was adjusted between 5 and 60 μg/mL. Devices were run in triplicate with running buffer containing either 0 or 50 ng/mL HA (11085-V08B, SinoBiological). The sample (100 μL) was added to the sample inlet, and when the devices were completed, the NC was removed and imaged with a smartphone (Motorola 1) under a lightbox containing 16 LEDs. Based on the analyzed results, a concentration of 40 μg/mL for anti-HA 2°Ab-HRP was chosen. For TMB optimization, the anti-HA 2°Ab-HRP was held constant at 40 μg/mL while the TMB volume was varied from 7.5 to 37.5 μL. Devices were run again in triplicate with 0 or 50 ng/mL HA, and 22.5 μL of TMB was chosen moving forward. For the CRP assay, a concentration of 20 μg/mL anti-CRP 2°Ab-HRP and a volume of 22.5 μL of TMB were chosen. These conditions worked considerably well for the CRP assay with little further optimization.

Multiplex Assay Operation. After HA assay conditions were optimized in the single-channel CaDI, dose−response curves for both assays were collected in the multiplex device. First, a range of HA concentrations was diluted in running buffer, and 160 μL of each concentration was added to the sample inlet of the multiplex device. The sample completely filled the channels and delivered the target to both NC test

https://doi.org/10.1021/acs.analchem.3c04977
Anal. Chem. 2024, 96, 4111−4119

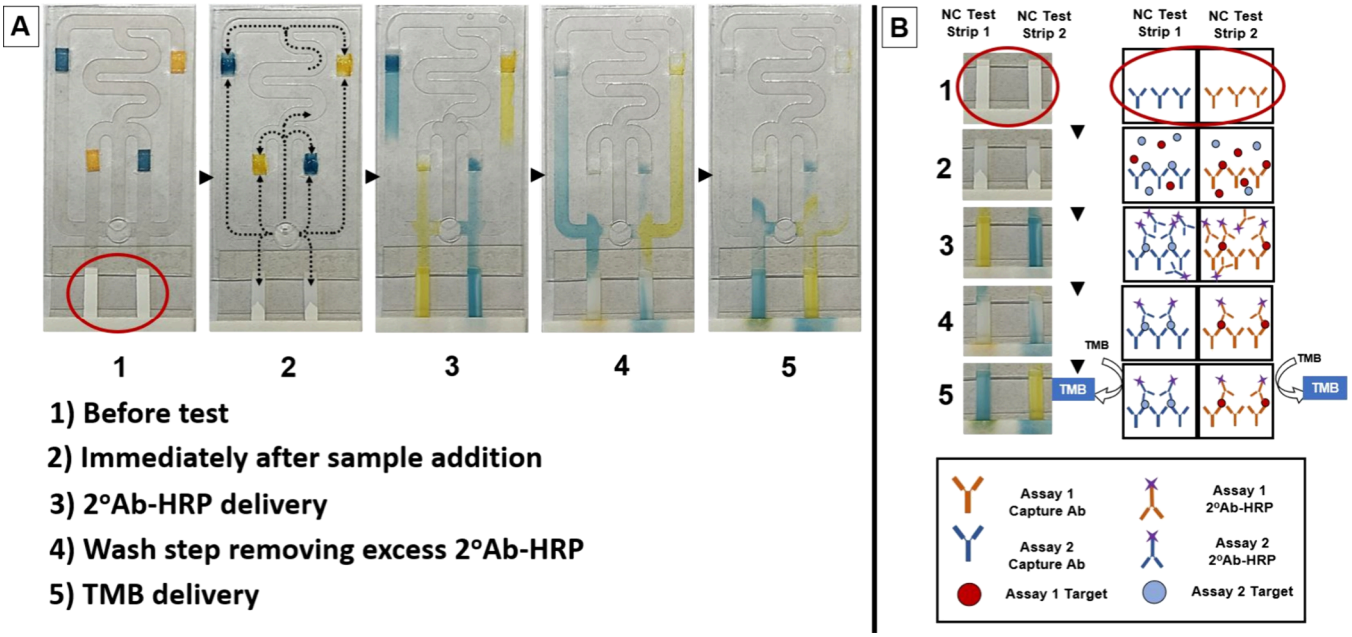

Figure 3. (A) The multiplex CaDI device function is broken down into five distinct key points. Image 1 depicts the device before the sample is added. Image 2 is immediately after the sample is added. The sample and buffer fill the channels (the direction of flow is depicted with gray arrows), and dried reagents are rehydrated. The target present flows through NC membranes and binds to the corresponding capture antibodies. In image 3, 2°Ab-HRP for each side of the device is delivered to its respective test strip. In image 4, excess 2°Ab-HRP is washed from each test strip. Last, in image 5, TMB is delivered to each test/control line, reacting with H_2O_2 in the buffer and HRP on the NC if present. (B) Images focused on the NC are accompanied by a molecular level schematic for each crucial step outlined in panel (A).

strips. Afterward, reagents for each side of the device were delivered passively to the NC membrane from the device via capillary action driven by the absorbent waste pad. The assay was completed when the buffer above the TMB pads was drained from the channels through the NC membrane, to the waste pad. After the assay was completed (<15 min), NC membranes were removed and allowed to dry for 5 min at RT before imaging with a Motorola 1 smartphone under the light box. The same procedures were performed with varying concentrations of N-protein spiked into running buffer. Devices were also run with 5 and 100 ng/mL for both targets simultaneously spiked into running buffer as a demonstration of simultaneous detection of two targets present in the same sample. As another example of simultaneous detection, 50 ng/mL for SARS-CoV-2 N-protein was added to running buffer already containing varying concentrations of CRP. One side of the multiplex device was prepared with the N-protein conjugate release pads and NC test strip, while the other contained reagents and NC for the CRP assay described above.

Image/Data Analysis. NC membranes were allowed to dry for 5 min at RT before being imaged under a light box. Images were uploaded to the free NIH software ImageJ. Images were converted to an 8-bit gray scale and inverted to provide a positive correlation with increasing target concentration. A rectangular area of interest was drawn around the area of the test line (or the blank area where the test line would be in the case of blank samples). A mean gray value measurement was taken of the test line area, and another measurement was taken in the area between the test line and the control line. The ratio of these values is called the "mean gray ratio" and was used for quantification purposes.

RESULTS AND DISCUSSION

Influenza Assay Optimization. The multiplex device used in this work consists of two separate immunoassays. Conditions for the N-protein assay had been optimized in previous work.[42] To optimize the HA assay, the single-channel CaDI device described previously was used, and the locations of conjugate release pads and NC membrane are shown in Figure 2A. Manufacturing the single-channel devices in bulk is slightly easier, giving us a quick way to determine the optimal 2°Ab-HRP concentrations and TMB volumes to use. First, the volume of TMB dried on the TMB pad was held constant at 30 μL while the concentration of 2°Ab-HRP dried was varied. The optimal concentration of 2°Ab-HRP was based on the results that gave the greatest signal for 50 ng/mL HA in running buffer and no signal with 0 ng/mL HA. The lowest concentration of 2°Ab-HRP where those criteria were met was 40 μg/mL. Despite having excess 2°Ab-HRP, more than 40 μg/mL did not improve the signal and had a slightly higher signal for the blank samples (Figure 2B). Next, 2°Ab-HRP was held constant at 40 μg/mL while the volume of the TMB substrate dried was varied. Devices were again run at 0 and 50 ng/mL HA. Although all TMB volumes above 15 μL performed similarly for signal intensity, 22.5 μL was chosen to ensure that an excess of TMB was present in the device (Figure 2B). Along with benefiting the multiplex device, this HA assay development is the first example in the literature of an automated, capillary-driven immunoassay for HA.

Multiplex Device Function and Theory. The optimized reagent pad conditions for the N-protein assay from previous work and for the HA assay described above were incorporated into the multiplexed microfluidic device. An NC test strip for each assay was inserted on its corresponding side, and the device was pressed down on an adhesive backing with a waste pad connected to the membrane. To operate the device, 160

https://doi.org/10.1021/acs.analchem.3c04977
Anal. Chem. 2024, 96, 4111−4119

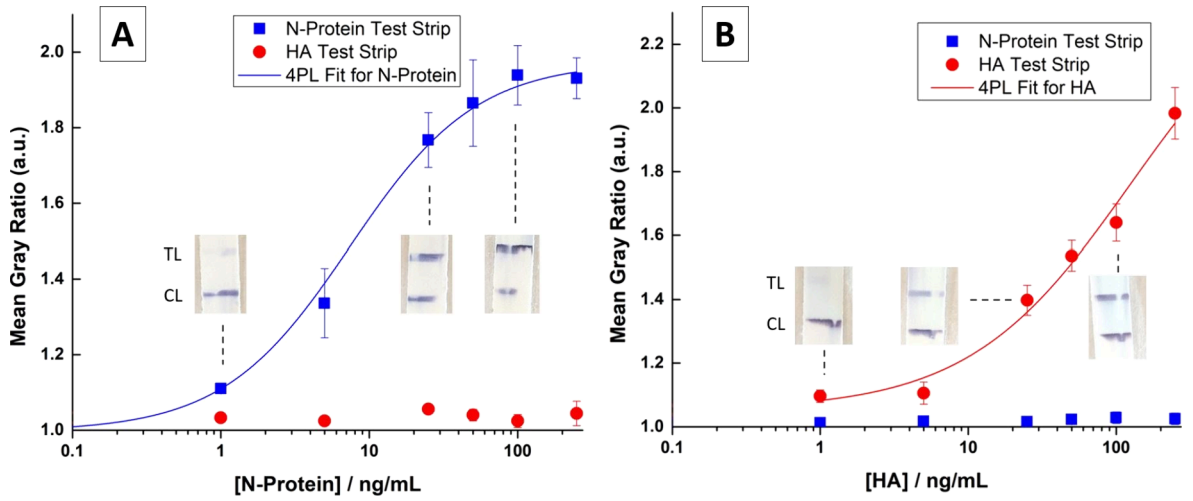

Figure 4. Dose−response curves were run for both targets separately, and representative images are shown for selected points showing the test line (TL) and control line (CL). (A) SARS-CoV-2 N-protein dose−response curve was run while holding the HA concentration at 0. The N-protein signal was fitted to a 4PL (R^2 = 0.98). (B) H1N1 HA dose−response was run, holding the N-protein concentration at 0. The signal for HA was fit to a 4PL fit (R^2 = 0.97).

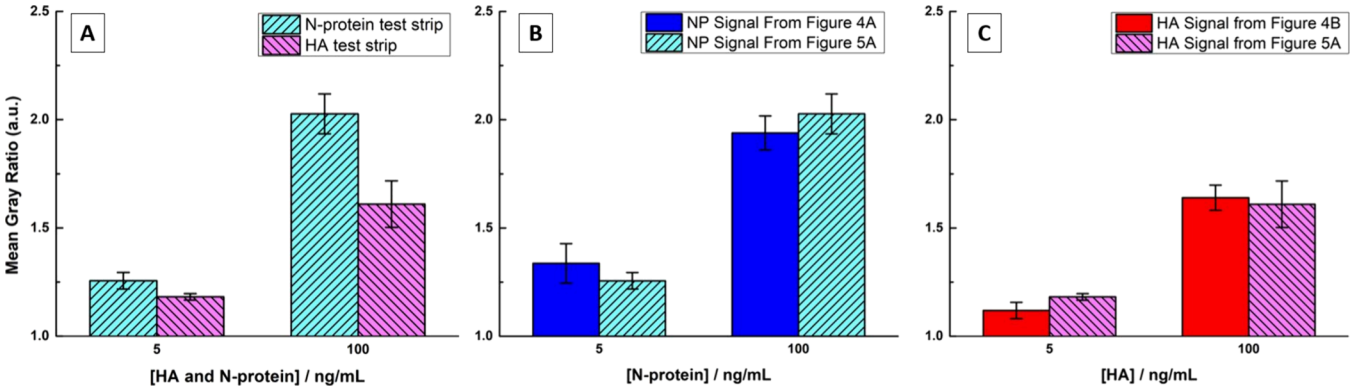

Figure 5. (A) Devices were run with 5 and 100 ng/mL for both HA and N-protein in running buffer simultaneously. (B) The N-protein data from panel (A) are compared to the signal intensity in Figure 4A when no HA is present in the running buffer. (C) The HA data from panel (A) are compared to the signal intensity from Figure 4B where no N-protein is present in running buffer.

μL of the sample is added to the sample inlet. No other end-user steps are required after the sample addition. When the sample is added, the solution fills the hollow channels in the device. The sample rehydrates 2°Ab-HRP and TMB from the conjugate release pads and flows through each NC membrane. If either target is present, then it will bind to the capture antibody stripped on its NC membrane. After this initial filling step, the buffer in the channels begins to drain into the waste pad through the capillary forces of the waste pad and the NC membranes. As the channels drain, an air bubble forms in the center channel above the sample inlet. Because of this air gap, 2°Ab-HRP from one side of the device cannot cross over to the other. 2°Ab-HRP is the next reagent delivered to the NC followed by a gap of sample buffer that washes any excess from the test lines. Last, TMB is delivered to each test line. The assay operation is shown in Figure 3A,B and Video S1 with blue and yellow food dye dried on the conjugate release pads to help visualize flow. Mismatched colors were chosen to show that there was no crossover from one side of the device to the other when reagents were delivered to the test strips. If the target is present at one or both test lines, then 2°Ab-HRP will also be present. TMB can with HRP and H_2O_2 in the running buffer form a solid blue test line. Control lines consisting of antimouse and antirabbit antibodies for NP and HA assays, respectively, should always be present.

Dose−Response Curves and Simultaneous Detection. Separate dose−response curves were gathered for both sides of the device. One target was diluted in running buffer containing hydrogen peroxide for the HRP reaction. The running buffer also contains NaCl for protein stability and surfactants to encourage release of reagents from the conjugate release pads, prevent nonspecific binding on the test lines, and to encourage uniform flow through the nitrocellulose, although some nonuniformity can be seen in the test lines. Varying concentrations of N-protein were run in triplicate with no HA present, and the resulting signal was fit to four-parameter logistic regression (4PL). The LOD for N-protein was determined to be three standard deviations above the signal of the blank sample, meaning that the LOD was 133 pg/mL. Ideally, regardless of the increase in the concentration of N-protein, the signal in the HA assay NC membrane should never be present if only N-protein is present in the sample. If that is the case, then a linear fit to the HA data should have a slope of 0. In this case, the slope of a linear fit to the HA signal was 0.00823 (Figure 4A). Additionally, an analysis of variance of the HA data shows that the points are indistinguishable

https://doi.org/10.1021/acs.analchem.3c04977
Anal. Chem. 2024, 96, 4111−4119

from each other with 95% confidence. The same procedures were done holding the N-protein concentration at 0 and varying the concentration of HA. For that data, the LOD of HA is 840 pg/mL, the slope of a linear fit for the N-protein side of the device is 0.00118, and the analysis of variance on the N-protein data showed that the points were indistinguishable with 95% confidence (Figure 4B).

Recent reports have shown that the coinfection of influenza and SARS-CoV-2 occurs in a significant number of cases.[56] To demonstrate the effectiveness of this multiplex device in detecting two analytes at the same time, HA and N-protein were spiked into running buffer. These samples containing both targets were run in triplicate, and the images for both sides of the devices were processed as described above (Figure 5A).

At both concentrations, a signal was present on both test strips after the samples had run. The resulting signal from Figure 5A was also compared to the signal that was obtained from the dose−response curve data in Figure 4 where only one target was present in the sample. With overlapping error bars and an analysis of variance, there is no significant difference in the signal between the data in Figures 4 and 5A (Figure 5B,C). This means that the presence of one target in the sample does not hinder the other side's ability to detect its intended target. Continuing to expand on multiplex applications, the simultaneous detection of SARS-CoV-2 and CRP was investigated next. Elevated levels of CRP in patients infected with SARS-CoV-2 have been correlated with worse patient outcomes.[53] Therefore, simultaneous diagnosis of a SARS-CoV-2 infection and quantification of CRP may help in the prognosis and treatment. Devices were assembled with SARS-CoV-2 reagents and test strip on one side and with CRP reagents and test strip on the other. Extraction buffer was spiked with varying concentrations of CRP as well as 50 ng/mL N-protein before running in the multiplex device. N-protein (50 ng/mL) represents a concentration at the high end of the dose−response in Figure 4A, and CRP concentrations were varied from 0 to 100 ng/mL (Figure 6). The presence of N-protein did not cause false positives on the CRP test strip, and the CRP test strip signal increased as the CRP concentration increased. Likewise, increasing the CRP concentration did not affect the signal present on the N-protein test strip, with an analysis of variance showing no statistical difference between the signal at any CRP concentration with >95% confidence. In this instance, the LEDs for the lightbox used to image were replaced before imaging, leading to a lighter background and a higher signal ratio on the N-protein side of the device compared with Figure 4. Ideally with this type of assay, health care providers would be able to determine if someone has a SARS-CoV-2 infection and how severe their symptoms may be based on quantification of CRP.

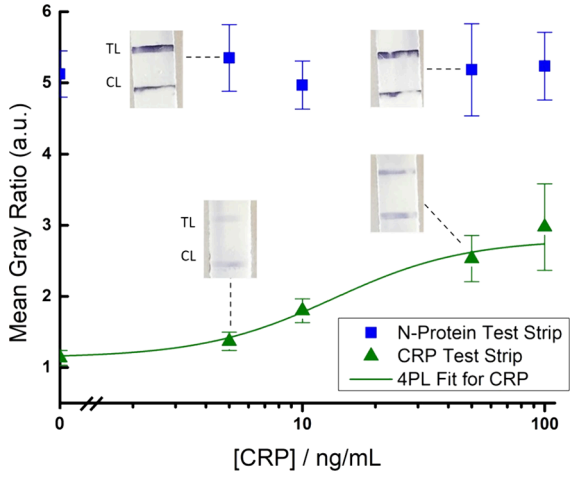

Figure 6. Devices were run with one side containing reagents and test strip for the N-protein immunoassay and the other side with reagents for the CRP assay. The CRP concentration was varied, while the N-protein concentration in the sample was held at 50 ng/mL. Representative images for each assay are included showing the location of the test line (TL) and control line (CL).

CONCLUSIONS

In this work, we show the first example of a multiplexed capillary-flow microfluidic ELISA in a POC-style device. Using hollow microfluidic channels, spatially separated NC test strips, and conjugate release pads, the device operates in a single sample addition step and outputs a visually detectable signal in under 15 min. The device can detect HA from H1N1 with an LOD of 840 pg/mL and N-protein from SARS-CoV-2 with an LOD of 133 pg/mL when spiked in running buffer. The device was initially designed with differentiation between SARS-CoV-2 and H1N1 infections in mind; the device can also be used for simultaneous detection of two targets. To demonstrate this concept, N-protein and HA were detected simultaneously as well as simultaneous detection of N-protein and CRP. This work demonstrates two important applications of multiplexed diagnostics: (i) distinguishing between conditions that may share similar symptoms and (ii) simultaneous detection of two targets for a more thorough analysis and future patient care. In all examples shown in this work, the signal is visible by the naked eye in under 15 min, and quantitative data can be determined using smartphone images. The effectiveness of simultaneous detection on this device and the spatial separation of the test strips point toward numerous future applications. Future work will aim to further multiplex the device, adding additional test lines to each test strip and increasing the number of targets that can be detected. Additionally, further device engineering, filtering steps, and buffer considerations will be made in the future to handle more complex biological samples.

ASSOCIATED CONTENT

Supporting Information

The Supporting Information is available free of charge at https://pubs.acs.org/doi/10.1021/acs.analchem.3c04977.

Video showing flow in the multiplexed microfluidic devices (MP4)

AUTHOR INFORMATION

Corresponding Author

Charles S. Henry − *Department of Chemistry and School of Biomedical Engineering, Colorado State University, Fort Collins, Colorado 80523, United States; Department of Chemical and Biological Engineering, Colorado State University, Fort Collins, Colorado 80523-1019, United States; Metallurgy and Materials Research Institute, Chulalongkorn University, Bangkok 10330, Thailand;* orcid.org/0000-0002-8671-7728; Email: chuck.henry@colostate.edu

https://doi.org/10.1021/acs.analchem.3c04977
Anal. Chem. 2024, 96, 4111−4119

Authors

Jeremy S. Link − *Department of Chemistry, Colorado State University, Fort Collins, Colorado 80523, United States*

John O'Donnell-Sloan − *Department of Chemical and Biological Engineering, Colorado State University, Fort Collins, Colorado 80523-1019, United States*

Sierra Curdts − *Department of Chemistry, Colorado State University, Fort Collins, Colorado 80523, United States*

Brian J. Geiss − *Department of Microbiology, Immunology and Pathology and School of Biomedical Engineering, Colorado State University, Fort Collins, Colorado 80523, United States*

David S. Dandy − *Department of Chemical and Biological Engineering, Colorado State University, Fort Collins, Colorado 80523-1019, United States; School of Biomedical Engineering, Colorado State University, Fort Collins, Colorado 80523, United States;* orcid.org/0000-0003-3254-0717

Complete contact information is available at: https://pubs.acs.org/10.1021/acs.analchem.3c04977

Notes

The authors declare no competing financial interest.

■ ACKNOWLEDGMENTS

Support for this work was provided by a grant from the National Institute of Health through the SPARK-REACH program (UO1-HL152405) and through R01AI132668 and R01EB031510. Additional support was provided by the National Science Foundation (NSF STTR 2032222).

■ REFERENCES

(1) Rasmussen, J.; Langerman, H. *Degenerative neurological and neuromuscular disease* **2019**, *9*, 123−130.

(2) Kashyap, D.; Kaur, H. *Life Sciences* **2020**, *246*, No. 117417.

(3) Bohunicky, B.; Mousa, S. A. *Nanotechnol., Sci. Appl.* **2011**, *4*, 1−10.

(4) Clinton, W. J. *New England Journal of Medicine* **2003**, *348* (18), 1800−1802.

(5) Gayle, H. D. *New England Journal of Medicine* **2003**, *348* (18), 1802−1805.

(6) Nitsche, A.; Schweiger, B.; Ellerbrok, H.; Niedrig, M.; Pauli, G. *Emerg Infect Dis* **2004**, *10* (7), 1300−1303.

(7) Al Hajjar, S.; McIntosh, K. *Ann. Saudi Med.* **2010**, *30* (1), 1−10.

(8) Otoo, J. A.; Schlappi, T. S. *Biosensors* **2022**, *12* (2), 124.

(9) Petti, C. A.; Polage, C. R.; Quinn, T. C.; Ronald, A. R.; Sande, M. A. *Clinical Infectious Diseases* **2006**, *42* (3), 377−382.

(10) Herd, G. C. E.; Musaad, S. M. A. *Archives of Pathology & Laboratory Medicine* **2021**, *145* (3), 327−335.

(11) Noviana, E.; Ozer, T.; Carrell, C. S.; Link, J. S.; McMahon, C.; Jang, I.; Henry, C. S. *Chem. Rev.* **2021**, *121* (19), 11835−11885.

(12) Omidfar, K.; Riahi, F.; Kashanian, S. *Biosensors* **2023**, *13* (9), 837.

(13) Sena-Torralba, A.; Álvarez-Diduk, R.; Parolo, C.; Piper, A.; Merkoçi, A. *Chem. Rev.* **2022**, *122* (18), 14881−14910.

(14) Jara, M. D. L.; Alvarez, L. A. C.; Guimarães, M. C. C.; Antunes, P. W. P.; de Oliveira, J. P. *Environmental science and pollution research international* **2022**, *29* (31), 46487−46508.

(15) Ngom, B.; Guo, Y.; Wang, X.; Bi, D. *Anal Bioanal Chem.* **2010**, *397* (3), 1113−1135.

(16) Chen, Y.; Chen, Q.; Han, M.; Zhou, J.; Gong, L.; Niu, Y.; Zhang, Y.; He, L.; Zhang, L. *Food Chem.* **2016**, *213*, 478−484.

(17) Tominaga, T. *J. Microbiol. Methods* **2019**, *160*, 29−35.

(18) Zhao, Y.; Wang, H.; Zhang, P.; Sun, C.; Wang, X.; Wang, X.; Yang, R.; Wang, C.; Zhou, L. *Sci. Rep.* **2016**, *6* (1), 21342.

(19) Yin, M.; Nie, Y.; Liu, H.; Liu, L.; Tang, L.; Dong, Y.; Hu, C.; Wang, H. *BMC Nephrology* **2022**, *23* (1), 30.

(20) Koczula, K. M.; Gallotta, A. *Essays Biochem* **2016**, *60* (1), 111−120.

(21) Peng, J.; Wang, Y.; Liu, L.; Kuang, H.; Li, A.; Xu, C. *RSC Adv.* **2016**, *6* (10), 7798−7805.

(22) Wang, Q.; Liu, Y.; Wang, M.; Chen, Y.; Jiang, W. *Anal. Bioanal. Chem.* **2018**, *410* (1), 223−233.

(23) Parolo, C.; Sena-Torralba, A.; Bergua, J. F.; Calucho, E.; Fuentes-Chust, C.; Hu, L.; Rivas, L.; Álvarez-Diduk, R.; Nguyen, E. P.; Cinti, S.; Quesada-González, D.; Merkoçi, A. *Nat. Protoc.* **2020**, *15* (12), 3788−3816.

(24) Ragavendar, M. S.; Anmol, C. M. *Annu. Int. Conf. IEEE Eng. Med. Biol. Soc.* **2012**, 2408−2411, DOI: 10.1109/EMBC.2012.6346449.

(25) Washburn, E. W. *Phys. Rev.* **1921**, *17* (3), 273−283.

(26) Gomez-Martinez, J.; Silvy, M.; Chiaroni, J.; Fournier-Wirth, C.; Roubinet, F.; Bailly, P.; Brès, J.-C. *Anal. Chem.* **2018**, *90* (12), 7502−7509.

(27) Taranova, N. A.; Byzova, N. A.; Zaiko, V. V.; Starovoitova, T. A.; Vengerov, Y. Y.; Zherdev, A. V.; Dzantiev, B. B. *Microchimica Acta* **2013**, *180* (11), 1165−1172.

(28) Dincer, C.; Bruch, R.; Kling, A.; Dittrich, P. S.; Urban, G. A. *Trends Biotechnol* **2017**, *35* (8), 728−742.

(29) Goldmann, F.; Bauer, N.; Moritz, A. *Comparative Clinical Pathology* **2014**, *23* (2), 283−296.

(30) Ernst, R.; Ogeer, J.; McCrann, D.; Cross, J.; Strong-Townsend, M.; Friis, H.; Coyne, M.; Clements, C.; Drake, C.; Murphy, R. *PLoS One* **2018**, *13* (10), No. e0205030.

(31) Hong, W.; Huang, L.; Wang, H.; Qu, J.; Guo, Z.; Xie, C.; Zhu, Z.; Zhang, Y.; Du, Z.; Yan, Y.; Zheng, Y.; Huang, H.; Yang, R.; Zhou, L. *J. Microbiol. Methods* **2010**, *83* (2), 133−140.

(32) Han, D. K.; Oh, J.; Lee, J.; Cho, Y. G.; Park, J. S.; Choi, J. S.; Kim, D. S.; Kwon, J. *Biosens. Bioelectron.* **2021**, *176*, No. 112894.

(33) Cheng, C.-M.; Martinez, A. W.; Gong, J.; Mace, C. R.; Phillips, S. T.; Carrilho, E.; Mirica, K. A.; Whitesides, G. M. *Angew. Chem., Int. Ed.* **2010**, *49* (28), 4771−4774.

(34) Fabiani, L.; Mazzaracchio, V.; Moscone, D.; Fillo, S.; De Santis, R.; Monte, A.; Amatore, D.; Lista, F.; Arduini, F. *Biosens. Bioelectron.* **2022**, *200*, No. 113909.

(35) Verma, M. S.; Tsaloglou, M.-N.; Sisley, T.; Christodouleas, D.; Chen, A.; Milette, J.; Whitesides, G. M. *Biosens. Bioelectron.* **2018**, *99*, 77−84.

(36) Carrell, C. S.; Wydallis, R. M.; Bontha, M.; Boehle, K. E.; Beveridge, J. R.; Geiss, B. J.; Henry, C. S. *RSC Adv.* **2019**, *9* (50), 29078−29086.

(37) Mu, X.; Zhang, L.; Chang, S.; Cui, W.; Zheng, Z. *Anal. Chem.* **2014**, *86* (11), 5338−5344.

(38) Samper, I. C.; Sánchez-Cano, A.; Khamcharoen, W.; Jang, I.; Siangproh, W.; Baldrich, E.; Geiss, B. J.; Dandy, D. S.; Henry, C. S. *ACS Sensors* **2021**, *6* (11), 4067−4075.

(39) Clark, K. M.; Schenkel, M. S.; Pittman, T. W.; Samper, I. C.; Anderson, L. B. R.; Khamcharoen, W.; Elmegerhi, S.; Perera, R.; Siangproh, W.; Kennan, A. J.; Geiss, B. J.; Dandy, D. S.; Henry, C. S. *ACS Measurement Science Au* **2022**, *2*, 584.

(40) Panraksa, Y.; Jang, I.; Carrell, C. S.; Amin, A. G.; Chailapakul, O.; Chatterjee, D.; Henry, C. S. *Anal. Methods* **2022**, *14*, 1774.

(41) CDC *Similarities and Differences between Flu and COVID-19*. 2022, https://www.cdc.gov/flu/symptoms/flu-vs-covid19.htm.

(42) Link, J. S.; Carrell, C. S.; Jang, I.; Barstis, E. J. O.; Call, Z. D.; Bellows, R. A.; O'Donnell-Sloan, J. J.; Terry, J. S.; Anderson, L. B. R.; Panraksa, Y.; Geiss, B. J.; Dandy, D. S.; Henry, C. S. *Anal. Chim. Acta* **2023**, *1277*, No. 341634.

(43) Shan, D.; Johnson, J. M.; Fernandes, S. C.; Suib, H.; Hwang, S.; Wuelfing, D.; Mendes, M.; Holdridge, M.; Burke, E. M.; Beauregard, K.; Zhang, Y.; Cleary, M.; Xu, S.; Yao, X.; Patel, P. P.; Plavina, T.; Wilson, D. H.; Chang, L.; Kaiser, K. M.; Nattermann, J.; Schmidt, S. V.; Latz, E.; Hrusovsky, K.; Mattoon, D.; Ball, A. J. *Nat. Commun.* **2021**, *12* (1), 1931.

(44) Anderson, C. E.; Holstein, C. A.; Strauch, E.-M.; Bennett, S.; Chevalier, A.; Nelson, J.; Fu, E.; Baker, D.; Yager, P. *Anal. Chem.* **2017**, *89* (12), 6608−6615.
(45) Chávez Ramos, K.; Nishiyama, K.; Maeki, M.; Ishida, A.; Tani, H.; Kasama, T.; Baba, Y.; Tokeshi, M. *ACS Omega* **2019**, *4* (15), 16683−16688.
(46) Wang, Z.; Zhao, Q.; Huang, M.; Duan, Y.; Li, F.; Wang, T. *Front. Microbiol.* **2022**, *13*, No. 934475, DOI: 10.3389/fmicb.2022.934475.
(47) Covin, S.; Rutherford, G. W. *Clinical Infectious Diseases* **2021**, *72* (12), e993−e994.
(48) Cuadrado-Payán, E.; Montagud-Marrahi, E.; Torres-Elorza, M.; Bodro, M.; Blasco, M.; Poch, E.; Soriano, A.; Piñeiro, G. J. *Lancet* **2020**, *395* (10236), No. e84.
(49) Kim, E.-H.; Nguyen, T.-Q.; Casel, M. A. B.; Rollon, R.; Kim, S.-M.; Kim, Y.-I.; Yu, K.-M.; Jang, S.-G.; Yang, J.; Poo, H.; Jung, J. U.; Choi, Y. K. *J. Virol.* **2022**, *96* (6), e01873−01821.
(50) Stowe, J.; Tessier, E.; Zhao, H.; Guy, R.; Muller-Pebody, B.; Zambon, M.; Andrews, N.; Ramsay, M.; Lopez Bernal, J. *International journal of epidemiology* **2021**, *50* (4), 1124−1133.
(51) Chen, N.; Zhou, M.; Dong, X.; Qu, J.; Gong, F.; Han, Y.; Qiu, Y.; Wang, J.; Liu, Y.; Wei, Y.; Xia, J. a.; Yu, T.; Zhang, X.; Zhang, L. *Lancet* **2020**, *395* (10223), 507−513.
(52) Gao, Y.; Li, T.; Han, M.; Li, X.; Wu, D.; Xu, Y.; Zhu, Y.; Liu, Y.; Wang, X.; Wang, L. *Journal of Medical Virology* **2020**, *92* (7), 791−796.
(53) Ali, N. *J. Med. Virol* **2020**, *92* (11), 2409−2411.
(54) Grant, B. D.; Anderson, C. E.; Williford, J. R.; Alonzo, L. F.; Glukhova, V. A.; Boyle, D. S.; Weigl, B. H.; Nichols, K. P. *Analytical chemistry* **2020**, *92* (16), 11305−11309.
(55) Ramachandran, S.; Fu, E.; Lutz, B.; Yager, P. *Analyst* **2014**, *139* (6), 1456−1462.
(56) Cong, B.; Deng, S.; Wang, X.; Li, Y. *J. Global Health* **2022**, *12*, No. 05040, DOI: 10.7189/jogh.12.05040.

https://doi.org/10.1021/acs.analchem.3c04977
Anal. Chem. 2024, 96, 4111−4119